ChemComm

COMMUNICATION

View Article Online
View Journal | View Issue

Cite this: *Chem. Commun.*, 2017, 53, 4985

Received 13th March 2017,
Accepted 3rd April 2017

DOI: 10.1039/c7cc01834g

rsc.li/chemcomm

Synthesis of SAPO-34 nanoaggregates with the assistance of an inexpensive three-in-one non-surfactant organosilane†

Pengfei Wu,[ab] Miao Yang,[a] Wenna Zhang,[ab] Shutao Xu,[a] Peng Guo,[a] Peng Tian*[a] and Zhongmin Liu *[a]

[3-Piperazinepropylmethyldimethoxysilane (PZPMS)] as a low-cost co-template, a crystal growth inhibitor, and a part of the silica source was used together with triethylamine to synthesize SAPO-34 nanoaggregates with tunable compositions. Note that the piperazinyl group of PZPMS prompts the formation of a perfect CHA structure by eliminating the CHA/AEI intergrowth, which ensures the excellent MTO catalytic performance of SAPO-34 nanoaggregates.

Silicoaluminophosphate (SAPO) molecular sieves are important solid acid catalysts.[1,2] In particular, SAPO-34 is a significant representative that shows good performance in the methanol-to-olefins (MTO) reaction due to its unique CHA structure, moderate acidity, and high hydrothermal stability. SAPO-34-based catalyst has been successfully applied in the commercialized MTO reactions since 2010.[3] However, circulating fluidized bed technology has to be adopted because SAPO-34 catalyst has a short catalytic lifetime, resulting from its diffusion limitation and fast coke deposition. It is, thus, highly desirable to retard the coking rate of SAPO-34 catalyst, which will increase the selectivity for light olefins and enhance the economic benefits of the MTO process.

Decreasing the crystal size and introducing mesopores into SAPO-34 are two effective solutions to improve the accessibility of the active sites, reduce the coking rate, and prolong the catalytic lifetime. Recently, amphiphilic quaternary ammonium-type organosilane surfactant has been demonstrated by our group and others to be effective for the synthesis of hierarchical SAPO-34.[4–7] However, the high cost of uncommon long-chain organosilane surfactant restricts its industrial application. Compared with the diverse mesoporogens or crystal growth inhibitors reported for the synthesis of aluminosilicate zeolites,[8,9] progress in SAPO molecular sieve systems remains rather limited. As is known, a bifunctional (micro- and mesopore) template is effective to achieve mesoporous zeolites as it avoids the phase separation of zeolites and mesoporous materials;[10–12] thus, it was hypothesized that multifunctional low-cost compounds, which direct the formation of the SAPO-34 framework, limit the crystal growth, and/or create mesoporosity, would be powerful and ideal for the synthesis of mesoporous or nanosized SAPO-34.

Due to this hypothesis, PZPMS, which is a commercial textile finishing agent that is widely used to treat cotton, flax, wool, and other artificial fibers,[13] attracted our attention. Interestingly, PZPMS simultaneously contains both piperazinyl and organosilane groups. The latter can be an effective silica source, whereas piperazine has been reported to act as a template for the CHA structure.[14] Thus, PZPMS is expected to have strong interactions with the SAPO framework, and it might act as a mesoporogen for the synthesis of SAPO-34.

Besides mesoporogen, the synthesis of hierarchical SAPO-34 strongly depends on the type of microporous template, which has significant effects on the product morphology, crystallinity, acidity, and thus on the MTO catalytic performance.[6] According to previous studies,[15] triethylamine (TEA) is not an ideal template for the synthesis of SAPO-34 although it is commercially available and cheap. This is because an intergrowth phase of SAPO-34(CHA)/18(AEI) with CHA as the majority product is generally obtained when TEA is used as a micropore template; moreover, the product always shows lower ethene plus propene selectivity in the MTO reaction. As the dimension of AEI cages (1.27 × 1.16 nm) in SAPO-18 is slightly larger than that of CHA cages (1.27 × 0.94 nm) in SAPO-34, it was speculated that the species and the concentration of the active intermediates formed in the AEI and CHA cages are different during the MTO reaction.[16,17] Therefore, it is important to avoid the AEI intergrowth while synthesizing the SAPO-34 catalyst.

Herein, we report a new low-cost tri-functional non-surfactant organosilane, PZPMS, for the first time to synthesize SAPO-34 under the assistance of triethylamine (TEA) template, in which PZPMS serves as a co-template, a crystal growth inhibitor, and a part silica source. The obtained SAPO-34 consisted of spherical agglomerates of nanocrystals with the pure CHA structure, large external surface, and tunable compositions. Note that the product

[a] *National Engineering Laboratory for Methanol to Olefins, Dalian National Laboratory for Clean Energy, Dalian Institute of Chemical Physics, Chinese Academy of Sciences, Dalian, 116023, China. E-mail: tianpeng@dicp.ac.cn, liuzm@dicp.ac.cn*

[b] *University of Chinese Academy of Sciences, Beijing, 100049, P. R. China*

† Electronic supplementary information (ESI) available. See DOI: 10.1039/c7cc01834g

Table 1 Synthesis conditions,[a] product phase, and composition

Sample	TEOS/Al_2O_3	PZPMS/Al_2O_3	Product composition	Product
SP34-M1	0.3	0	$Si_{0.084}Al_{0.490}P_{0.426}O_2$	SAPO-34/18+ impurity
SP34-M2	0.3	0.2	$Si_{0.101}Al_{0.484}P_{0.414}O_2$	SAPO-34
SP34-M3	0.3	0.4	$Si_{0.121}Al_{0.481}P_{0.398}O_2$	SAPO-34
SP34-M4	0.3	0.6	—	Amorphous
SP34-M5[b]	0.12	0.4	$Si_{0.087}Al_{0.502}P_{0.411}O_2$	SAPO-34
SP34-P[c]	0.32	0	$Si_{0.088}Al_{0.495}P_{0.417}O_2$	SAPO-34
SP34-C[d]	—	—	$Si_{0.086}Al_{0.484}P_{0.430}O_2$	SAPO-34/18

[a] The initial gel molar composition: Al_2O_3/P_2O_5/TEOS/PZPMS/TEA/H_2O = 1.0/1.0/*x*/*y*/4.5/100 (200 °C, 24 h). [b] Adding 5% amount of milled SAPO-34 as seeds into the initial gel. [c] Adding piperazine as co-micropore template together with TEA, *n*(PIP) : *n*(TEA) = 0.4 : 4.5. [d] Pseudoboehmite used as an Al source and alkaline silica sol as a Si source, the initial gel molar composition: $Al_2O_3/P_2O_5/SiO_2$/TEA/H_2O = 1.0/1.0/0.4/3.0/50 (200 °C, 24 h).

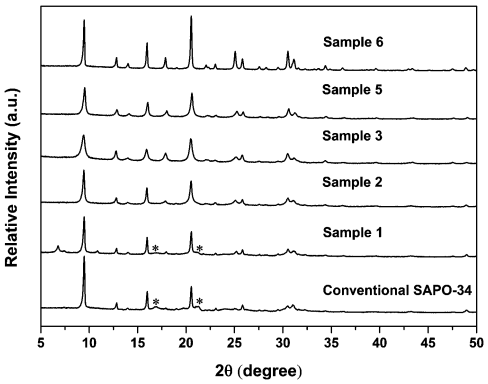

Fig. 1 XRD patterns of the as-synthesized samples. Asterisks indicate the AEI phase.

exhibits prolonged MTO catalytic lifetime, reduced coking rate, and higher selectivity for light olefins compared with the conventional SAPO-34.

A series of SAPO-34 samples was prepared by introducing different amounts of PZPMS. The sample was designated as SP34-Mx. A small amount of SAPO-34 seed was introduced, if necessary, for widening the crystallization phase region. For comparison, SAPO-34 samples were also synthesized using TEA as the single template (SP34-C) and with piperazine as the co-template (SP34-P). The experimental results are listed in Table 1.

According to the product crystallinity and morphology, the optimal composition ratio can be summarized as follows: Al_2O_3/P_2O_5/TEOS/PZPMS/TEA/H_2O = 1.0/1.0/0.3/0.4/4.5/100. When the TEOS/Al_2O_3 ratio was lower than 0.3 and PZPMS was absent, the product was contaminated by a minor impurity. With the addition of PZPMS, the impurity disappeared possibly due to its silica source role as high Si content in the initial gel facilitates the synthesis of pure SAPO-34.[18] XRF analysis further confirms our speculation. It shows a gradual increase in the Si contents of the products from SP34-M1 to SP34-M3 with the increase of PZPMS. Since the dosage of TEOS is constant, the increased Si content should be contributed by PZPMS. However, the synthesis of SAPO-34 cannot be achieved using PZPMS as the only silica source. Each PZPMS has only two methoxysilane groups, which may be insufficient for the formation of the CHA structure. Even in the presence of TEOS, an amorphous phase is the final product (SP34-M4) when the PZPMS/Al_2O_3 ratio is higher than 0.6. It suggests that too much PZPMS inhibits the crystal growth. To promote crystallization and widen the phase region, a small amount of SAPO-34 seed was introduced such that the Si content of the product could be modified. SP34-M5, with a lower Si content, was achieved, and the related data is listed in Table 1.

The XRD patterns of the as-synthesized and calcined samples are displayed in Fig. 1 and Fig. S1 (ESI†), respectively. For the sample SP34-M1, the XRD pattern is a little complicated and contains additional weak diffraction peaks at 7.5, 7.8, 16.9, and 21.3 (2θ degree) besides the peaks belonging to SAPO-34. After calcinations, the peaks at 7.5 and 7.8 (2θ degree) disappeared. It indicates that there was an impurity of the unstable phase, whose ordered structure collapsed after calcination. Moreover, the peaks at 16.9 and 21.3 (2θ degree) suggest the presence of the intergrowth of SAPO-18 with SAPO-34.[19] The DIFFaX program was used to simulate the XRD patterns of the SAPO-18/34 intergrowth phase with different SAPO-34 and SAPO-18 ratio. Referring to the simulated patterns shown in Fig. S1 (ESI†), the content of SAPO-18 in calcined SP34-C was evaluated to be around 20%. Interestingly, upon the addition of PZPMS, the peaks originating due to the impurity and intergrowth phase disappeared, implying that PZPMS can modify the crystalline phase of the product. In addition to the change in the XRD peak position, the XRD patterns became broad as the PZPMS content was increased, especially obvious for SP34-M3 and SP34-M5, showing decrease in the particle size.

SEM images (Fig. 2a–d and Fig. S2, ESI†) show the change in the product morphology with the increase of PZPMS in the initial gel. The primary particle size of the samples decreased with the addition of PZPMS. Note that SP34-M3 and SP34-M5 presented a spherical aggregate morphology with the average particle size of about 1 μm, which consist of small cubic crystals of 100–200 nm size (Fig. 2c), indicating that the addition of PZPMS can restrain the growth of the crystals. N_2 adsorption isotherms and pore size distribution of the samples are depicted in Fig. 2e and f. The texture results are given in Table S1 (ESI†). SP34-M3 gives a type I plus IV isotherm with a hysteresis loop in the $0.5 < P/P_0 < 0.8$ region. The BJH mesopore size distribution of SP34-M3 based on the adsorption branch is dominant at 3.8 nm, which should result from the inter-crystal pores of the nanoparticles. The isotherm of SP34-M5 shows an obvious increase with a hysteresis loop after $P/P_0 > 0.7$. The mesopore size distribution of SP34-M5 is centered at 11 nm. In comparison with the samples synthesized without the use of PZPMS, the samples SP34-M3 and SP34-M5 exhibit a larger external surface area and higher mesopore volume (Table S1, ESI†), which would facilitate the diffusion and mass transport of molecules in the catalytic reactions.

To investigate the incorporation of PZPMS and the local Si atomic environments, solid-state ^{13}C and ^{29}Si NMR spectra were obtained for SP34-M5. The ^{13}C MAS NMR spectrum is shown in Fig. 3(a). The two strong resonance peaks at 48.3 and 9.2 ppm can be undoubtedly attributed to the methylene and methyl groups of TEA template,[20] whereas the other small peaks near

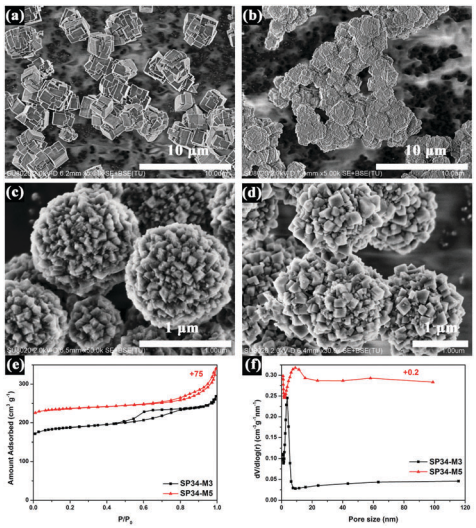

Fig. 2 SEM images of the calcined SP34-M1 (a), SP34-M2 (b), SP34-M3 (c), and SP34-M5 (d), and N_2 sorption isotherms (e) and pore size distributions (f) of SP34-M3 and SP34-M5.

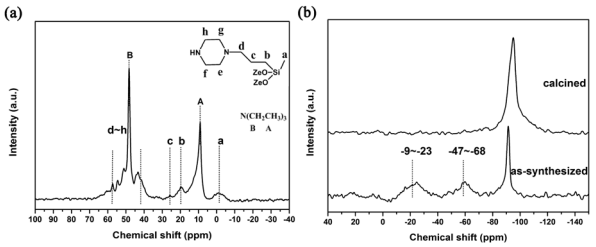

Fig. 3 (a) ^{13}C MAS NMR spectrum of the as-synthesized SP34-M5, (b) ^{29}Si CP MAS NMR spectrum of the as-synthesized SP34-M5 and ^{29}Si MAS NMR spectrum of the calcined SP34-M5.

48.3 ppm can be attributed to the piperazinyl (e, f, g, and h) and methylene groups (d) connected to the N atom of PZPMS. The two resonance peaks at 26.0 and 19.8 ppm correspond to the other two methylene groups adjacent to methoxysilane (c and b, respectively), and the peak at −2 ppm is ascribed to the methyl group linked to methoxysilane.[21] These results confirm the incorporation of PZPMS into the SAPO-34 crystals. The ^{29}Si CP MAS NMR spectrum of the as-synthesized SP34-M5 is shown in Fig. 3(b). The sharp resonance peak centered at −92 ppm is ascribed to the $Si(OAl)_4$ species. The broad signal between −9 and −23 ppm could be attributed to the D_n groups (D_n = $RR'Si(OAl)_n(OH)_{2-n}$, n = 1 and 2), indicating that the organosiloxane groups of PZPMS are condensed into the SAPO-34 framework.[22] In addition, there is another broad signal from −47 to −68 ppm corresponding to the T_n' signals (T_n' = $RSi(OAl)_n(OH)_{3-n}$, n = 2 and 3).[6,23] It suggests that parts of the Si–C bonds of PZPMS might be broken during the crystallization process. After calcination, the resonances from D_n and T_n groups disappeared due to the removal of organics.

TG-DTA and elemental analyses were carried out to evaluate the introduced amount of organic species in the samples. As seen in Fig. S3 and Table S2 (ESI†), the weight loss increased and the C/N ratio decreased with the increase in the PZPMS/Al_2O_3 ratio.

Previous literature has reported that piperazine is a type of template that can direct the structure of CHA. It is, thus, supposed that the piperazinyl group of PZPMS might serve as a co-template to affect the phase formation. A contrast synthesis with mixed templates of TEA and piperazine was also carried out to synthesize SAPO-34 (SP34-P). The XRD result (Fig. 1) gives a typical CHA diffraction pattern without any intergrowth phase, verifying the role of the piperazinyl group of PZPMS in inhibiting the formation of the SAPO-34/18 intergrowth.

To understand the existing statutes of PZPMS, density functional theory (DFT) calculation was used to investigate the interaction energy between implanted PZPMS and H-SAPO-34. A possible position of PZPMS in CHA structure was simulated and calculated using the Gaussian09 package.[24] First, the organosilanes undergo hydrolysis as shown in the following equation:

$$RR'Si(OCH_3)_2 + 2H_2O \rightarrow RR'Si(OH)_2 + 2CH_3OH$$

Then, the hydrolyzed PZPMS connects with the SAPO framework forming ZeO-SiRR′ (I) and ZeO-SiRR′(OH) (II) structures. The optimized structures are shown in Fig. 4, where the piperazinyl group is confined in one CHA cage, while the other part of PZPMS stays in the adjacent CHA cage. A possible situation in the real reaction might be that the piperazinyl group acts as the co-template and stays in the CHA cage, while the propylmethyldimethoxysilane tail slows down the crystal growth of SAPO-34, which favors the formation of nanoparticle aggregates through a surface interaction. The interaction energies between PZPMS and SAPO-34 were calculated to be −471.8 for structure I and −174.6 kcal mol^{-1} for structure II, indicating that the existence of PZPMS itself could stabilize the SAPO-34 framework, especially in structure I. When TEA is put in the cage together with PZPMS, the interaction energies show a slight decrease from −471.8(I)/−174.6(II) to −476.4(I)/−189.1(II) kcal mol^{-1} due to the synergetic combination of TEA and PZPMS.

Combining the above mentioned results, it can be concluded that PZPMS plays a triple function in the synthesis of SAPO-34. The propylmethyldimethoxysilane group of PZPMS acts as a part of the silica source and simultaneously inhibits the crystal growth, while the piperazinyl group of PZPMS plays as a co-template to suppress the intergrowth of the AEI/CHA phase.

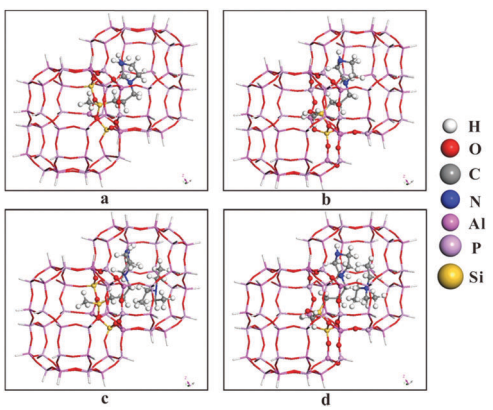

Fig. 4 The optimized geometry structures of condensed PZPMS. (a) ZeO-SiRR′, (b) ZeO-SiRR′(OH), (c) ZeO-SiRR′ + TEA, and (d) ZeO-SiRR′(OH) + TEA.

Table 2 Lifetime[a] and product distribution[b] of samples in the MTO reaction (WHSV = 2 h^{-1}, T = 450 °C)

Sample	Lifetime (min)	$C2^=$ (%)	$C3^=$ (%)	$C2^= + C3^=$ (%)	$C2^=/C3^=$ (%)	Coke content[c] (%, g g_{cat}^{-1})	R_{coke}[c] (mg min^{-1})
SP34-M5	376	50.00	33.65	83.65	1.49	25.19	0.064
SP34-P	191	49.85	34.71	84.56	1.43	21.41	0.112
SP34-C	208	43.25	37.17	80.42	1.16	20.65	0.099

[a] Catalyst lifetime is defined as the reaction duration with >99% methanol conversion. [b] Based on the highest selectivity of ethene and propene under >99% methanol conversion. [c] Determined using a TG and DTA analyzer up to 800 °C measured after the MTO reaction.

The MTO catalytic properties of the samples with relatively low and comparable Si content were evaluated at 450 °C with a methanol WHSV of 2 h^{-1}. The results are summarized in Table 2 and Table S3 and Fig. S4 (ESI†). SP34-M5 exhibits the longest catalytic lifetime of 376 min and relatively high ethene plus propene selectivity of 83.65%. Comparatively, the lifespan of microporous SP34-C and SP34-P are only 208 min and 191 min, respectively. NH_3-TPD measurements were conducted to evaluate the catalyst acidity, and the results are shown in Fig. S5 (ESI†). All the samples show similar acid strength, whereas the acidic concentration for SP34-M5 is slightly lower than those of SP34-C and SP34-P. It is, thus, believed that the prolonged lifespan and obviously lower coke deposition rate (Table 2) of SP34-M5 is due to the lower acidic concentration and reduced crystal size, which shortens the diffusion paths and enhances the mass transfer efficiency during the MTO reaction.

Interestingly, it can be seen in Table 2 that the selectivity of ethene plus propene and the $C2^=/C3^=$ ratio of the MTO product catalyzed by pure SAPO-34 samples (SP34-M5 and SP34-P) are obviously higher than those of the intergrowth phase (SP34-C). Given that spatial confinement effects may affect the active intermediates and product selectivity, we further examined the hydrocarbon species retained in the catalysts during the MTO reaction. SP34-P and SP34-C with comparable crystal particle size were selected for the investigation such that the possible influence of diffusion limitation could be avoided. As some organic intermediates are too active to be captured at 450 °C, the MTO reaction was conducted at 350 °C. More experimental details are given in the ESI.†

The GC-MS results obtained after 40 min MTO reaction are shown in Table S4 and Fig. S6 (ESI†). There are similar carbon species including multi-methylbenzenes, naphthalene, and methylnaphthalene in SP34-C and SP34-P catalysts. However, it is apparent from Table S4 (ESI†) that the proportion of highly substituted methylbenzenes (pentamethylbenzene and hexamethylbenzene) is much higher in SP34-C (25.7%) than that in SP34-P (12.4%). It has been reported that methylbenzenes with two or three methyl groups preferentially yield ethene, whereas penta- and hexamethylbenzene favor propene generation during the MTO reaction.[25] Thus, it is believed that SP34-C containing both the CHA and larger AEI cages provides more space for the accommodation of highly substituted methylbenzenes than pure SAPO-34 (SP34-P), which thus results in different product selectivity over the catalysts.

In summary, using a low-cost commercial non-surfactant organosilane, PZPMS, SAPO-34 nanoaggregates with excellent MTO catalytic performance were synthesized and characterized. The triple function of PZPMS in the synthesis ensures its powerful effect on the product morphology and crystal phase. It is expected that more multifunctional compounds having strong interactions with the SAPO framework will be developed for the synthesis of hierarchical or nanosized SAPO molecular sieves.

This work was supported by the National Natural Science Foundation of China (21476228, 21676262) and the Key Research Program of Frontier Sciences, CAS (QYZDB-SSW-JSC0 40).

References

1 R. Yadav and A. Sakthivel, *Appl. Catal., A*, 2014, **481**, 143–160.
2 J. Shi, Y. Wang, W. Yang, Y. Tang and Z. Xie, *Chem. Soc. Rev.*, 2015, **44**, 8877–8903.
3 P. Tian, Y. Wei, M. Ye and Z. Liu, *ACS Catal.*, 2015, **5**, 1922–1938.
4 M. Choi, H. S. Cho, R. Srivastava, C. Venkatesan, D. H. Choi and R. Ryoo, *Nat. Mater.*, 2006, **5**, 718–723.
5 Q. Sun, N. Wang, D. Xi, M. Yang and J. Yu, *Chem. Commun.*, 2014, **50**, 6502–6505.
6 C. Wang, M. Yang, P. Tian, S. Xu, Y. Yang, D. Wang, Y. Yuan and Z. Liu, *J. Mater. Chem. A*, 2015, **3**, 5608–5616.
7 C. Wang, M. Yang, M. Li, S. Xu, Y. Yang, P. Tian and Z. Liu, *Chem. Commun.*, 2016, **52**, 6463–6466.
8 D. P. Serrano, J. Aguado, J. M. Escola, J. M. Rodriguez and A. Peral, *J. Mater. Chem.*, 2008, **18**, 4210–4218.
9 D. P. Serrano, J. Aguado, J. M. Escola, J. M. Rodriguez and A. Peral, *Chem. Mater.*, 2006, **18**, 2462–2464.
10 J. Zhu, Y. Zhu, L. Zhu, M. Rigutto, A. van der Made, C. Yang, S. Pan, L. Wang, L. Zhu, Y. Jin, Q. Sun, Q. Wu, X. Meng, D. Zhang, Y. Han, J. Li, Y. Chu, A. Zheng, S. Qiu, X. Zheng and F. Xiao, *J. Am. Chem. Soc.*, 2014, **136**, 2503–2510.
11 Y. Yuan, P. Tian, M. Yang, D. Fan, L. Wang, S. Xu, C. Wang, D. Wang, Y. Yang and Z. Liu, *RSC Adv.*, 2015, **5**, 9852–9860.
12 M. Choi, K. Na, J. Kim, Y. Sakamoto, O. Terasaki and R. Ryoo, *Nature*, 2009, **461**, 246–249.
13 Q. An, C. Li, H. Li and X. Li, *China Pat.*, CN105694062, 2016.
14 N. Li, H. Zhao, Y. Ding and S. Xiang, *China Pat.*, CN201210337437.5, 2015.
15 C. Wang, M. Yang, W. Zhang, X. Su, S. Xu, P. Tian and Z. Liu, *RSC Adv.*, 2016, **6**, 47864–47872.
16 J. Chen, J. Li, Y. Wei, C. Yuan, B. Li, S. Xu, Y. Zhou, J. Wang, M. Zhang and Z. Liu, *Catal. Commun.*, 2014, **46**, 36–40.
17 J. Li, Y. Wei, J. Chen, S. Xu, P. Tian, X. Yang, B. Li, J. Wang and Z. Liu, *ACS Catal.*, 2015, **5**, 661–665.
18 B. Gao, M. Yang, Y. Qiao, J. Li, X. Xiang, P. Wu, Y. Wei, S. Xu, P. Tian and Z. Liu, *Catal. Sci. Technol.*, 2016, **6**, 7569–7578.
19 R. L. Smith, W. A. Sławiński, A. Lind, D. S. Wragg, J. H. Cavka, B. Arstad, H. Fjellvåg, M. P. Attfield, D. Akporiaye and M. W. Anderson, *Chem. Mater.*, 2015, **27**, 4205–4215.
20 D. Fan, P. Tian, S. Xu, Q. Xia, X. Su, L. Zhang, Y. Zhang, Y. He and Z. Liu, *J. Mater. Chem.*, 2012, **22**, 6568–6574.
21 Q. Mei, B. Tong, L. Liang and M. Lu, *J. Photochem. Photobiol., A*, 2007, **191**, 216–221.
22 P.-Y. Mabboux and K. K. Gleason, *J. Electrochem. Soc.*, 2005, **152**, F7–F13.
23 Z. Zhang, B. P. Gorman, H. Dong, R. A. Orozco-Teran, D. W. Mueller and R. F. Reidy, *J. Sol-Gel Sci. Technol.*, 2003, **28**, 159–165.
24 A. Dkhissi, A. Estève, L. Jeloaica, M. D. Rouhani and G. Landa, *Chem. Phys.*, 2006, **323**, 179–184.
25 W. Song, H. Fu and J. F. Haw, *J. Am. Chem. Soc.*, 2001, **123**, 4749–4754.

